Inorg. Chem. **2005**, *44*, 3844–3849

$Ni_{11}As_8$ Single-Crystalline Nanosheets via Hydrothermal Redox Route

Shuo Wei, Jun Lu, Weichao Yu, Houbo Zhang, and Yitai Qian*

Structure Research Laboratory and Department of Chemistry,University of Science and Technology of China.Hefei, Anhui, 230026, People's Republic of China

Received November 5, 2004

$Ni_{11}As_8$ crystallites 23-nm thick and 250–700-nm wide in lateral dimension were prepared in alkaline hydrothermal condition. Transmission electron microscope (TEM) images and selected area electron diffraction (SAED) analyses showed that the as-prepared $Ni_{11}As_8$ was single-crystalline nanosheets of [331] orientation. The $Ni_{11}As_8$ exhibited an optical absorption onset of 3.00 eV in the visible spectral regime. Its magnetic measurement indicated a weak magnetic hysteresis and unsaturation magnetization with a magnetic susceptibility of 1.37×10^{-4} cm^3/g (at 15 kOe) at room temperature, the origin of which was discussed and assigned to the effect of surface species containing Ni ions. The extended Hückel tight-binding calculation revealed that bulk $Ni_{11}As_8$ has a 3d-localized narrow band below Fermi level and complicated band structure with small band gap in the first Brillouin zone, which supply clues to explain the observed optical and magnetic properties. The formation mechanism of $Ni_{11}As_8$ was studied and attributed to an alkaline hydrothermal redox route on the basis of the Marsh reaction.

I. Introduction

In the past decades, there has been considerable attention in the low-dimensional semiconductor materials, including the two-dimensional (2D) quantum wells (QWs), and 1D nanowires. The reduced size and large surface-to-volume ratios result in new electronic, optical, and magnetic properties (e.g., quantum size effect) which differ from those of their bulk counterparts. For example, 2D semiconductor structures are important model systems for studying quantum coherences in electron plasmas and optical polarization control.[1−4] The quantum confinement of electrons along the *z* direction leads to the formation of sub-bands, between which dipole-allowed optical inter-sub-band transitions occur at frequencies determined by the QW width.[5] On the other hand, many layered materials including clay minerals,[6] graphite oxides,[7] layered double hydroxides,[8] and layered transition-metal oxides[9−12] are candidates for quasi 2D systems, which may have varied properties compared with bulk materials because of 1D size confinement of the crystalline dimensions. Their successful preparations enriched the 2D materials family and provide possibility to discover more novel chemical and physical properties and potential applications in semiconductor devices[13] and photocatalysis.[14] Recently, many transition-metal oxides 2D unilamellar colloids were characterized by chemical delamination meth-

* Author to whom correspondence should be addressed. E-mail: ytqian@ustc.edu.cn.

(1) Monroe, C. *Nature (London)* **2002**, *416*, 238.
(2) Heyman, J. N.; Kersting, R.; Unterrainer, K. *Appl. Phys. Lett.* **1998**, *72*, 644.
(3) Eickemeyer, F.; Woerner, M.; Weiner, A. M.; Elsaesser, T.; Hey, R.; Ploog, K. H. *Appl. Phys. Lett.* **2001**, *79*, 165.
(4) Capasso, F.; Gmachl, C.; Sivco, D. L.; Cho, A. Y. *Phys. Today* **2002**, *55*, 34.
(5) Luo, C. W.; Reimann, K.; Woerner, M.; Elsaesser, T.; Hey, R.; Ploog, K. H. *Phys. Rev. Lett.* **2004**, *92*, 047402.
(6) Nadeau, P. H.; Wilson, M. J.; McHardy, W. J.; Tait, J. M. *Science* **1984**, *225*, 923.
(7) (a) Kovtyukhova, N. I.; Ollovier, P. J.; Martin, B. R.; Mallouk, T. E.; Chizhik, S. A.; Buzaneva, E. V.; Gorchinsky, A. D. *Chem. Mater.* **1999**, *11*, 771. (b) Cassagneau, T.; Fendler, J. H. *Adv. Mater.* **1998**, *10*, 877.
(8) (a) Adachi-Pagano, M.; Forano, C.; Besse, J.-P. *Chem. Commun.* **2000**, 91. (b) Hibino, T.; Jones, W. *J. Mater. Chem.* **2001**, *11*, 1321.
(9) (a) Wang, L. Z.; Omomo, Y.; Sakai, N.; Fukuda, K.; Nakai, I.; Ebina, Y.; Takada, K.; Watanabe, M.; Sasaki, T. *Chem. Mater.* **2003**, *15*, 2873. (b) Omomo, Y.; Sasaki, T.; Wang, L. Z.; Wanatabe, M. *J. Am. Chem. Soc.* **2003**, *125*, 3568.
(10) (a) Wang, L.; Sasaki, T.; Ebina, Y.; Kurashima, K.; Watanabe, M. *Chem. Mater.* **2002**, *14*, 4827. (b) Sasaki, T.; Ebina, Y.; Fukuda, K.; Tanaka, T.; Harada, M.; Watanabe, M. *Chem. Mater.* **2002**, *14*, 3524.
(11) (a) Sasaki, T.; Watanabe, M. *J. Am. Chem. Soc.* **1998**, *120*, 4682. (b) Sasaki, T.; Watanabe, M.; Hashizume, H.; Yamada, H.; Nakazawa, H. *J. Am. Chem. Soc.* **1996**, *118*, 8329. (c) Sukpirom, N.; Lerner, M. M. *Chem. Mater.* **2001**, *13*, 2179. (d) Unal, U.; Matsumoto, Y.; Tanaka, N.; Kimura, Y.; Tamoto, N. *J. Phys. Chem. B* **2003**, *107*, 12680.
(12) (a) Miyamoto, N.; Nakato, T. *Adv. Mater.* **2002**, *14*, 1267. (b) Xu, F. F.; Ebina, Y.; Bando, Y.; Sasaki, T. *J. Phys. Chem. B* **2003**, *107*, 6698.
(13) (a) Matsumoto, Y.; Funatsu, A.; Matsuo, D.; Unal, U.; Ozawa, K. *J. Phys. Chem. B* **2001**, *105*, 10893. (b) Koinuma, M.; Seki, H.; Matsumoto, Y. *J. Electroanal. Chem.* **2002**, *531*, 81.
(14) Kim, Y. I.; Samer, S.; Huq, M. J.; Mallouk, T. E. *J. Am. Chem. Soc.* **1991**, *113*, 9561.

10.1021/ic048448e CCC: $30.25
Published on Web 04/21/2005

ods, among which a compound with a layered crystal lattice was disintegrated into the constitute single layers, include unilamellar MnO_2 exfoliated from $H_{0.13}MnO_2 \cdot 0.7H_2O$,[9] TiO_2 monolayer from layered titanates $H_xTi_{2-x/4}O_4 \cdot H_2O$,[10,11] and $[Nb_6O_{17}^{4-}]$ layer from $K_4Nb_6O_{17}$.[12] Some well-crystalline lamellar crystallites with nonlayered lattice such as single-crystalline ZnO (thicknesses of 30−70 nm)[15] and Ga_2O_3 sheets (cleavage plane of (100))[16] were prepared by thermal oxidation of ZnS and GaN, respectively. However, so far very few investigations have been reported on non-oxide 2D structures, except for NiS[17] and ZnS.[18]

As a type of important non-oxides, transition-metal pnictides ME (M = Co, Ni; and E = P, As) have been served as alternative Schottky and ohmic contact layers of III−V group semiconductors thin films or devices for they exhibit metallic properties combined with a diffusion-limiting pnictides content.[19] However, few studies on Ni−As compounds such as NiAs, $NiAs_2$, and $Ni_{11}As_8$ have been reported thus far. It has been known that maucherite ($Ni_{11}As_8$) is not nearly so common as niccolite (NiAs) in natural hydrothermal deposits and natural maucherite is found associated with niccolite (NiAs), rammelsbergite ($NiAs_2$), and pararammelsbergite ($NiAs_2$) in nickel−cobalt-native silver deposits.[20] Synthetic $Ni_{11}As_8$ crystallites were previously obtained by elemental direct reaction in evacuated sealed tube at 700∼825 °C with a lengthy preparation period of 30 days. Structure analysis shows that it has a large complex tetragonal supercell (a = 6.872 Å, c = 21.82 Å, space group $P4_12_12$) containing 44 Ni and 32 As atoms, where Ni atoms have six nonequivalent positions, therein, five Ni atoms are square pyramidal coordination with As, one has a stretched octahedral coordination with As, and the As polyhedra form single chains of trigonal prisms.[21] Other reports on properties on $Ni_{11}As_8$ are rather rare, and no electron band structure study was published until now.

In This Paper, we report a novel and convenient method for the preparation of $Ni_{11}As_8$ crystallites in aqueous ammonia at 190 °C. The as-prepared $Ni_{11}As_8$ are nanosheets 23-nm thick and 250−700-nm wide in lateral size and single-crystalline with [331] preferred orientation. To gain further insight into the physical properties of these lamellar crystallites, we carried out optical and magnetic measurements, and an extended Hückel calculation attempt was made to understand these properties by analysizing the band structure of bulk $Ni_{11}As_8$. The hydrothermal reaction mechanism of Ni−As_2O_3 system was also studied to explain the formation of $Ni_{11}As_8$ in ammonia.

II. Experimental Section

All chemicals were of analytical grade and were purchased from Shanghai Chemical Reagents Company. In a typical hydrothermal procedure, metal nickel (99.99%, 0.294 g, 5 mmol) and excessive arsenous oxide (As_2O_3, 99%, 0.495 g, 5 mmol, ***CAUTION:*** great care should be taken when using toxic As_2O_3) were mixed into 50 mL of aqueous ammonia (25−28 vol %, pH > 14); after being stirred completely, the reactant solution was transferred into a stainless Teflon-lined autoclave of 60 mL which was sealed and maintained at 190 °C for 12−24 h, and then the autoclave was cooled to room temperature naturally. The gray solid was separated by filtration and washed repeatedly with distilled water, diluted hydrochloric acid, and anhydrous ethanol. Finally, the product was dried in a vacuum at 60 °C for 2 h.

Powder X-ray diffraction (XRD) pattern was measured on a MXP 18 AHF X-ray diffractometer (MAC Science Co. Ltd., Japan) equipped with graphite-monochromatized Cu Kα X-ray (λ = 1.54184 Å) with a scanning rate of 8 °min^{-1}. Before measurement of powder XRD pattern, the samples were levigated into fine powders by an agate mortar and pestle to minimize preferred orientation. Indexing and lattice constants refinements were carried out by a PC software program TREOR90.[22,23] Scanning electron microscope (SEM) images and energy-dispersive X-ray fluorescence (EDX) analysis were taken on a JEOL JSM-6700F field emission scanning electron microscope operated at 10 kV. High-resolution transmission electron microscope (HRTEM) images and selected area electron diffraction (SAED) pattern were obtained using a JEOL 2010 transmission electron microscope at an acceleration voltage of 200 kV. Room-temperature optical absorption measurements of the $Ni_{11}As_8$ product ultrasonically dispersed in methanol were performed in a 1-cm quartz cuvette using a Shimadzu UV365 UV/vis/NIR spectrophotometer. The magnetic measurements of the samples were carried out in a vibrating sample magnetometer (VSM) (BHV-55, Riken Denshi Co. Ltd, Japan) with a maximal applied magnetic field of 15 kOe. Seventy-three milligrams of the as-prepared $Ni_{11}As_8$ was filled into a plastic sample chamber of 66.05 μL and sealed for measurement. The scanning speed of magnetic field was set as 3 min per loop. Magnetization curves were recorded at 283 K by first magnetizing the powder sample in a field of 15 kOe; then, the remanent magnetization (M_r), and the coercivity (H_c) were determined. The magnetization curve of metal nickel was also measured to compare with that of $Ni_{11}As_8$.

The semiempirical extended Hückel tight-binding method[24] was employed to calculate the band structure of bulk $Ni_{11}As_8$ in which 10 valence electrons per Ni atom and 5 per As were considered and the following orbital exponents (ζ) and valence shell ionization potentials (H_{ii} in eV) were used in the calculation:[25] As 4s ζ 2.23, H_{ii} −16.22; As 4p ζ 1.89, H_{ii} −12.16; Ni 4s ζ 2.10, H_{ii} −10.95; Ni 4p ζ 2.10, H_{ii} −6.27; Ni 3d H_{ii} −14.20; Ni 3d orbital was represented by sums of two exponents: ζ_1 = 5.75 with the weighting coefficient c_1 = 0.5493 and ζ_2 = 2.30 with c_2 = 0.6082. A 40 k-point set was used in average property calculations on bulk $Ni_{11}As_8$.

(15) (a) Hu, J. Q.; Bando, Y.; Zhan, J. H.; Li, Y. B.; Sekiguchi, T. *Appl. Phys. Lett.* **2003**, *83*, 4414. (b) Tian, Z. R. R.; Voigt, J. A.; Liu, J.; McKenzie, B.; McDermott, M. J.; Rodriguez, M. A.; Konishi, H.; Xu, H. F. *Nat. Mater.* **2003**, *2*, 821.
(16) (a) Dai, Z. R.; Pan, Z. W.; Wang, Z. L. *J. Phys. Chem. B* **2002**, *106*, 902. (b) Gundiah, G.; Govindaraj, A.; Rao, C. N. R. *Chem. Phys. Lett.* **2002**, *351*, 189.
(17) Chen, D. L.; Gao, L.; Zhang, P. *Chem. Lett.* **2003**, *32* 996.
(18) (a) Yang, J.; Xue, C.; Yu, S. H.; Zeng, J. H.; Qian, Y. T. *Angew. Chem., Int. Ed.* **2002**, *41*, 4697. (b) Yu, S. H.; Yoshimura, M. *Adv. Mater.* **2002**, *14*, 296.
(19) Williams, R. S. *Appl. Surf. Sci*, **1992**, *60/61*, 613.
(20) Fleet, M. E. *Am. Mineral.* **1973**, *58*, 203.
(21) Yund, R. A. *Ecol. Geol.* **1961**, *56*, 1273.
(22) Werner, P. W. *Z. Kristallogr.* **1964**, *120*, 375.
(23) Werner, P. W.; Eriksson, L.; Westdahl, M. *J. Appl. Crystallogr.* **1985**, *18*, 367.
(24) Landrum, G. A.; Glassey, W. V. Yet Another Extended Hückel Molecular Orbital Package (Yaehmop, including bind 3.0 and viewkel 3.0). Yaehmop is freely available on the WWW at http://sourceforge.net/projects/yaehmop/.
(25) *Tables of Parameters for Extended Hückel Calculations*; collected by Alvarez, S. Universitat de Barselona, Spain 1993.

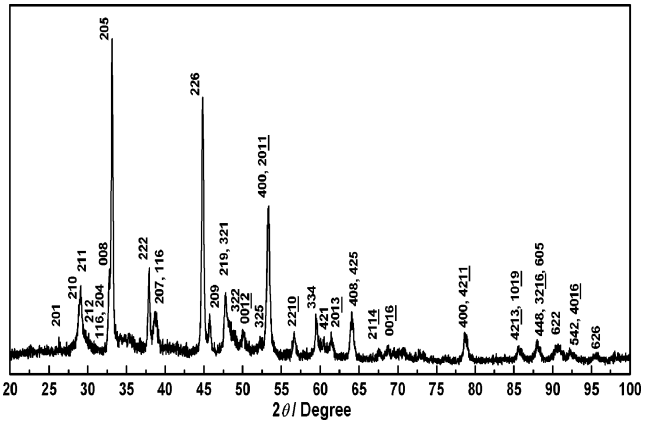

Figure 1. Powder XRD pattern of $Ni_{11}As_8$ sheets.

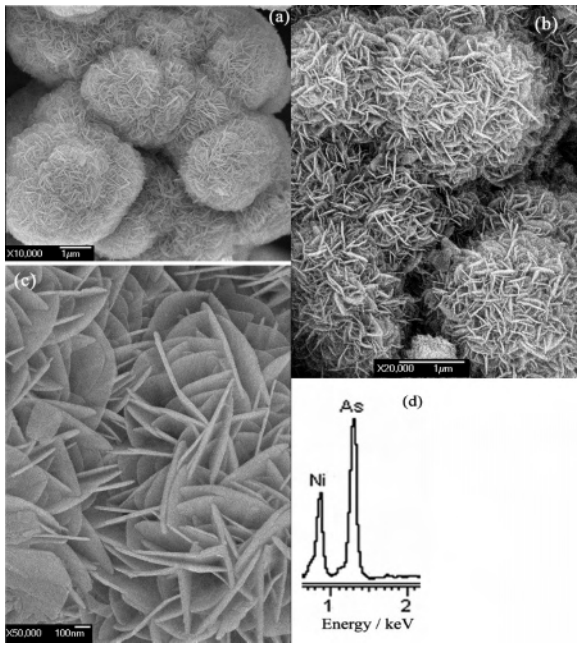

Figure 2. SEM images (a−c) and EDX spectrum (d) of $Ni_{11}As_8$ nanosheets.

III. Results and Discussion

Powder XRD, Morphology, and Crystalline Orientation. The phase of hydrothermal product was characterized by powder X-ray diffraction. As shown in Figure 1, all diffraction peaks were indexed as a tetragonal lattice of $Ni_{11}As_8$ ($a = 6.8704 \pm 2 \times 10^{-4}$Å, $c = 21.8157 \pm 5 \times 10^{-4}$Å) with a high figure of merit (for a typical sample, $F_{30} = 27$)[26] which are close to the reference data.[27] No other crystalline impurities including elements (Ni or As), oxides (arsenic oxides or arsenous oxides), $Ni(OH)_2$, NiAs, and $NiAs_2$ are detected by XRD, which indicate that pure $Ni_{11}As_8$ can be obtained via this hydrothermal method.

Figure 2 shows the SEM images of as-prepared $Ni_{11}As_8$ products. In Figure 2a and 2b, spherical secondary particles with 2−6 μm in diameter can be found, which reveal that they consist of fine lamellar microcrystals. Figure 2c unambiguously shows that these microcrystals are uniform sheets with thickness of 23 nm in average and lateral dimension of 250−700 nm (630 nm in average). EDX (Figure 2d) analysis on these secondary particles indicates that the molar ratio of Ni:As is 57.93:42.07 (=1.377:1) which is consistent with the stoichiometry of $Ni_{11}As_8$.

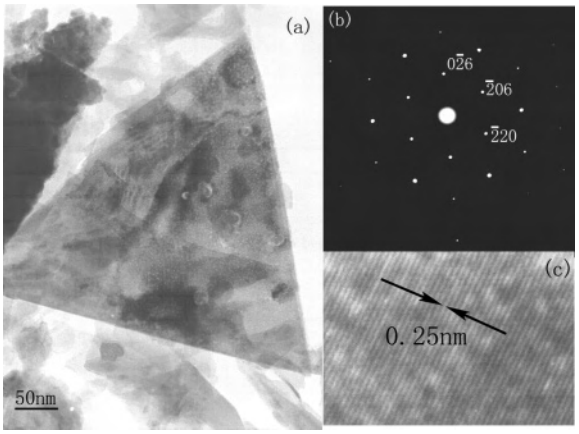

Figure 3. TEM image (a), SAED pattern (b), and lattice fringes image (c) of a $Ni_{11}As_8$ nanosheet.

The crystalline orientation of individual sheet was investigated by high-resolution transmission electron microscopy (HRTEM). Figure 3a is the TEM image of a typical triangular $Ni_{11}As_8$ sheet with a side of 500 nm; its SAED pattern (Figure 3b) shows single-crystalline diffraction dots with hexagonal symmetry at first glance. After careful measurement, it is found that the ED pattern is pseudohexagonal, which can be regarded as belonging to [331] zone axis of tetragonal $Ni_{11}As_8$ lattice if it is approximatively viewed as a threefold cubic superlattice along *c* axis (the axis ratio $c/a = 3.175$).[28] The high-resolution image (Figure 3c) reveals parallel fringes with a space of 0.25 nm, which is consistent with the space of (220) or (206) lattice planes. Therefore, it could be concluded that the as-prepared $Ni_{11}As_8$ are single-crystalline nanosheets with [331] preferred orientation. Taking the average thickness of 23 nm into account, the sheets have only six periods in the [331] direction (the lattice period in the [331] direction is 3.64 nm).

Optical Absorption Spectroscopy. Figure 4 shows room-temperature optical absorption spectrum of the as-prepared $Ni_{11}As_8$ sheets; a featureless absorption rise dominates the absorption spectrum in the range of visible and near-infrared region. The absorption onset was estimated to be 3.00 eV (415 nm). The onset of 3.00 eV cannot be undoubtedly assigned to be a band gap, and we assume $Ni_{11}As_8$ sheets as direct band gap semiconductors; by employing the plot of $(Ah\nu)^2 \sim h\nu$ to get a band gap E_g of direct band gap semiconductors,[29] a gap of 3.45 eV (360 nm) can be obtained (Figure 4 inset). No mater which onset, it implied that the

(26) Smith, G. S.; Synder, R. L. *J. Appl. Crystallogr.* **1979**, *12*, 60.
(27) Joint Committee on Powder Diffraction Standards (JCPDS), File No. 76-881, $Ni_{11}As_8$, tetragonal system, space group $P4_12_12$, $a = 6.8724(4)$ Å, $c = 21.821(1)$ Å, $c/a = 3.1752$; therein, *d* spaces were calculated.
(28) $d_{220} = 2.4297$, $d_{206} = 2.4977$ Å, the angle between them is 60.895°, which is very approximate to the 60° for true hexagonal symmetrical ED pattern.
(29) For $h\nu > E_g$, the formula is $Ah\nu = B(h\nu - E_g)^{1/2}$, therein *A* is the absorbance, $h\nu$ is the absorption energy, E_g is the direct band gap, and *B* is a constant relative to the material; therefore, the E_g of $Ni_{11}As_8$ can be determined by extrapolating the curve of $(Ah\nu)^2 \sim h\nu$.

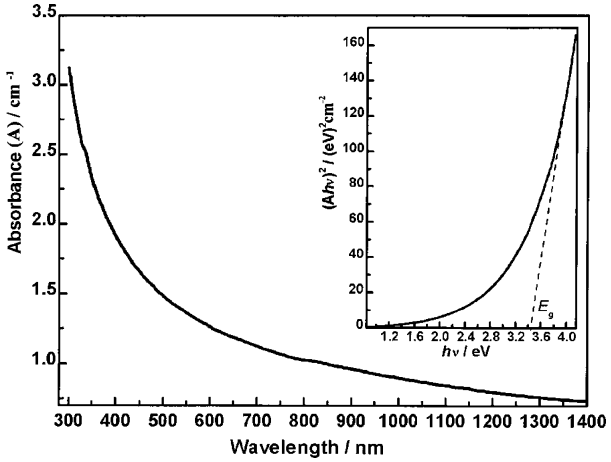

Figure 4. Optical absorption spectrum of $Ni_{11}As_8$ sheets and a plot of $(Ah\nu)^2 \sim h\nu$ to obtain a possible direct band gap E_g (inset).

$Ni_{11}As_8$ sheets has an absorption character in visible spectral regime which is similar to many semiconducting oxide nanosheets with a blueshift of band gap.[30] It can be expected that the electron confinement in [331] direction modified the energy band structure, which resulted in the visible absorption character of $Ni_{11}As_8$ nanosheets.

Magnetic Measurement. The room-temperature magnetization curve of $Ni_{11}As_8$ sheets shown in Figure 5a exhibits a slight hysteresis loop, a character of weak ferromagnetic behavior. The coercivity (H_c) and remanent magnetization (M_r) is 312 Oe and 0.0192 emu/g, respectively (Figure 5b). The susceptibility by mass χ_g (at 15 kOe) is 1.37×10^{-4} cm^3/g (or 1.51×10^{-3} by volume). Notice from the magnetization curve that the magnetization is far from saturation up to the highest field applied of 15 kOe, which implies either a saturation magnetization occurs at higher applied field (>15 kOe) or no saturation can be observed.

This weak hysteresis and unsaturation magnetization of $Ni_{11}As_8$ sheets is different from that of nonmagnetic bulk counterpart (maucherite) and also different from metal nickel which is a typical ferromagnetic metal and has a saturation magnetization at about 5 kOe.[31] Unsaturation magnetization has been reported in small magnetically ordered systems such as $NiFe_2O_4$ and $CoFe_2O_4$ and has been attributed to a noncollinear spin structure due to surface-spin pinning effect.[32] On the other hand, some $Ni(OH)_2$ and NiO nanocrystals have been reported to show ferromagnetism at low temperature (<10 K).[33] Therefore, the weak hysteresis and unsaturation magnetization of the 2D $Ni_{11}As_8$ sheets can be temporarily assigned to a surface effect related to surface species containing Ni ions. In the view of the fact that the $Ni_{11}As_8$ sheets have only six periods in the [331] direction, this surface influence on magnetization behavior cannot be neglected. An in-depth study including temperature dependence of susceptibility and surface species analysis will be needed to clarify the origin of magnetic behavior of $Ni_{11}As_8$ sheets.

Calculated Band Structure of Bulk $Ni_{11}As_8$. The extended Hückel calculation[31] gives the density of state (DOS) plot of bulk $Ni_{11}As_8$ (shown in Figure 6) and implies the bulk $Ni_{11}As_8$ is metallic and has a Fermi level (E_F) of −11.40 eV with small DOS immediately above E_F. A remarkable character in the DOS plot is that there is a narrow band centered at −14.10 eV below the E_F which can be viewed as the contribution of Ni atoms because the projected DOS of Ni atoms (light-gray hatching in Figure 6) almost fills all of the total DOS narrow band. This energy of DOS maximum is slightly greater than the ionization potential of Ni 3d electron (−14.20 eV) which indicates that this narrow band localizes in the Ni 3d atomic orbitals. Since the Ni atoms have unpaired 3d electrons which are also localized in $Ni_{11}As_8$ tetragonal lattice, it is possible that the localized electron configuration is one of the factors of the observed weak ferromagnetic behavior in the $M-H$ curve.[34]

On the other hand, the calculation also gave a complicated band structure (Figure 7). At the Brillouin zone origin (Γ), there is a small energy gap with 0.55 eV, and the states immediately above the Fermi level result from Ni 4s orbitals (−10.95 eV). A similar energy gap also occurred in the Brillouin border at point Z (0.7 eV), A (0.5 eV), and even in the preferred orientation [331] direction of nanosheets (Y, 0.3 eV). In view of the nanoscale of $Ni_{11}As_8$ in [331] direction, one can expect two factors for the 3.0 eV absorption onset: one is that it originates from high-energy level transitions since there are abundant empty bands available above Fermi level and another is that it derives from the bulk energy gaps in the Brillouin zone which were enlarged because of the quantum confinement effect.

These speculations on magnetic and optical absorption spectra were all based on the extended Hückel calculation and therefore are primary and temporary. More experimental study (e.g., electron conductivity measurement, ultraviolet photoelectron spectra) is very necessary to verify the calculated DOS plots and band structures.

Hydrothermal Formation Mechanism. A reaction mechanism study on the $Ni-As_2O_3$ hydrothermal system was carried out and the results are summarized in Table 1, from which it can be concluded that, in neutral hydrothermal condition, no reaction occurs, and arsenide can only be obtained in either acidic or alkaline solution. $Ni_{11}As_8$ is the stable phase in alkaline hydrothermal condition; in acidic aqueous solution, however, the same reactants give NiAs product as a hydrothermal stable phase.[31] Furthermore, in acidic condition, metastable $Ni_{11}As_8$ is an intermediate product, which decomposes into NiAs within an extended reaction period. It has been reported that maucherite melts incongruently to niccolite at 830 °C;[21] in our acidic system, however, this hydrothermal-aided decomposition occurred at a much lower temperature (190 °C). Therefore, in a hydrothermal system, it follows that the alkaline solution

(30) Sasaki, T.; Watanabe, M. *J. Phys. Chem. B* **1997**, *101*, 10159.
(31) For more details, see Supporting Information.
(32) (a) Kodama, R. H.; Berkowitz, A. E.; McNiff, E. J.; Foner, S. *Phys. Rev. Lett.* **1996**, *77*, 394. (b) Haneda, K.; Morrish, A. H. *J. Appl. Phys.* **1988**, *63*, 4258.
(33) Ichiyanagi, Y.; Wakabayashi, N.; Yamazaki, J.; Yamada, S.; Yoshihide, Y.; Komatsu, E.; Tajima, H. *Physica B* **2003**, *329−333*, 862.
(34) Oledzka, M.; Lee, J.-G.; Ramanujachary, K. V.; Greenblatt, M. *J. Solid State Chem.* **1996**, *127*, 151.

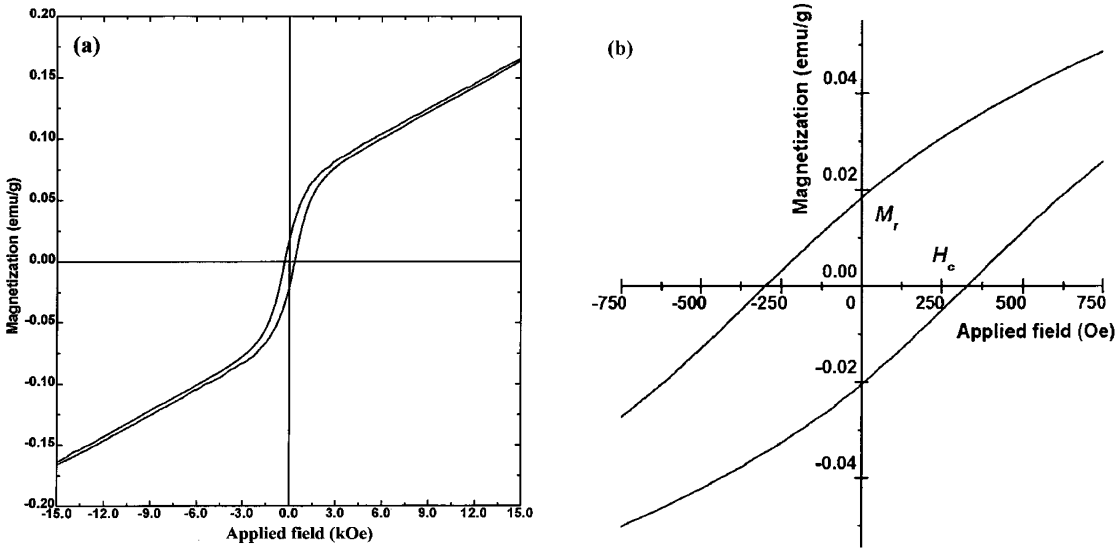

Figure 5. (a) Magnetization vs applied magnetic field for the $Ni_{11}As_8$ sheets at 283 K and (b) the enlarged low field regime of (a) to obtain the M_r and H_c.

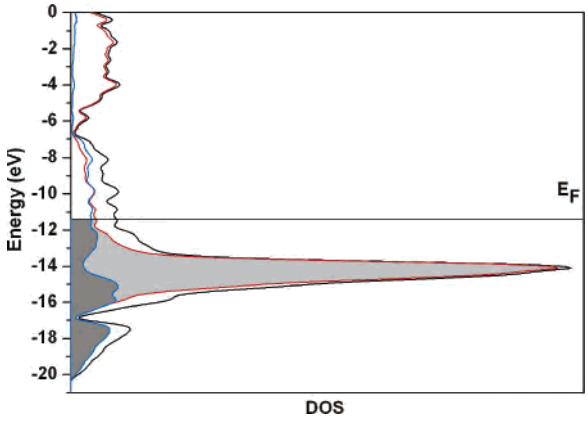

Figure 6. The calculated total DOS (black line), projected Ni (red line, light-gray shading), and As DOS (blue line, gray shading). E_F: Fermi energy level.

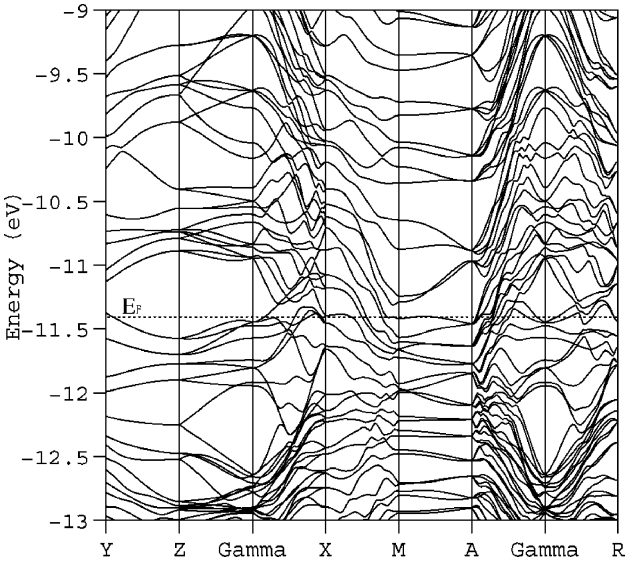

Figure 7. The calculated band structure of bulk $Ni_{11}As_8$ along selected symmetry lines in the first Brillouin zone; E_F: Fermi energy level. Γ (0, 0, 0), X (0.5, 0, 0), Z (0, 0, 0.5), M (0.5, 0.5, 0), A (0.5, 0.5, 0.5), R (0.5, 0, 0.5), Y (1/6, 1/6, 1/2)

stablizes the square pyramidal coordination phase of $Ni_{11}As_8$ (10 out of 11 Ni atoms), which, in acidic condition, further releases Ni^{2+} into the solution to reach the higher octahedral coordination of NiAs. Our previous work indicates that GaAs nanocystals could be obtained by substituting zinc with gallium in the Marsh reaction, a routine method for determining arsenic, which utilizes metal zinc to reduce arsenates or arsenites in acidic solution.[35] The current results show that, similar to gallium, nickel can also reduce As_2O_3 in acidic or alkaline solution and results in NiAs and $Ni_{11}As_8$, respectively. This implies that, according to this route, it is possible to prepare other metal arsenides in hydrothermal condition.

IV. Conclusion

In conclusion, $Ni_{11}As_8$ single-crystalline sheets of 23-nm thick and 250−700 nm in lateral dimension have been prepared in alkaline hydrothermal condition. TEM images and SAED analysis show the single-crystalline sheets are of [331] orientation. The $Ni_{11}As_8$ sheets exhibit an optical absorption onset of 3.00 eV in the visible spectral regime. Their magnetization curve shows a weak magnetic hysteresis and unsaturation magnetization at room temperature with a magnetic susceptibility of 1.37×10^{-4} cm^3/g (15 kOe); taking the 2D morphology of sheets into account, this magnetic behavior can be assigned to the effect of surface species containing Ni. The extended Hückel tight-binding calculation points out that bulk $Ni_{11}As_8$ has a 3d-localized narrow band below Fermi level and complicated band

Table 1. The Hydrothermal Product of Redox Reaction: Ni + As_2O_3

solvent	190 °C, 9 h	190 °C, 15 h
HCl (1 M)	NiAs, $Ni_{11}As_8$	NiAs[a]
H_2O	Ni	Ni
$NH_3 \cdot H_2O$	$Ni_{11}As_8$, Ni	$Ni_{11}As_8$

[a] When $Ni_{11}As_8$ is hydrothermally treated in HCl (1 M) at 190 °C for 12 h, NiAs can also be obtained exclusively.[31]

(35) (a) Wei, S.; Lu, J.; Yu, W. C.; Zhang, H. B., Qian, Y. T. *Chem. Lett.* **2004**, *33*, 386. (b) Lu, J.; Wei, S.; Yu, W. C.; Zhang, H. B., Qian, Y. T. *Inorg. Chem.* **2004**, *43*, 4543.

structure with small band gap in Γ, A, and Z points in Brillouin zone, which supply potential explanations on the observed optical and magnetic properties. The formation mechanism of $Ni_{11}As_8$ is attributed to a hydrothermal redox route based on the Marsh reaction, which revealed that $Ni_{11}As_8$ and NiAs are stable phases in alkaline and acidic hydrothermal conditions, respectively. This redox route is also applied into preparation of other metal arsenide crystallites. It can be concluded that these single-crystalline $Ni_{11}As_8$ nanosheets provide a novel 2D system to study dimensional-related properties (e.g., quantum confinement, magnetic) of transition-metal arsenides.

Acknowledgment. This work was supported by the National Natural Science Foundation of China and the National Key Fundamental Research and Development Program of China (973 Program).

Supporting Information Available: The $M-H$ curve of metal Ni, the XRD patterns, and the SEM image of the products via the acidic hydrothermal reaction and the calculation details of the energy band structure of $Ni_{11}As_8$. These materials are available free of charge via the Internet at http://pubs.acs.org.

IC048448E